

Electronic structure effects from hydrogen bonding in the liquid phase and in chemisorption: an integrated theory and experimental effort

Lars G. M. Pettersson,^{a*} Anders Nilsson,^b Satish Myneni,^c Yi Luo,^a Mats Nyberg,^a Matteo Cavalleri,^a Lars Ojamäe,^d Lars-Åke Näslund,^b Hirohito Ogasawara,^b Michael Odelius^d and Alexander Pelmeshnikov^a

^aFYSIKUM, University of Stockholm, Box 6730, S-113 85 Stockholm, Sweden, ^bPhysics Department, University of Uppsala, Box 530, S-751 21 Uppsala, Sweden, ^cDepartment of Geosciences, Princeton University, Princeton, NJ 08544, USA, ^dPhysical Chemistry, Arrhenius Laboratory, Stockholm University, S-106 91 Stockholm, Sweden, and ^ePhysical Chemistry, Uppsala University, Box 532, S-751 21 Uppsala, Sweden. E-mail: lgm@physto.se

A closely integrated theoretical and experimental effort to understand chemical bonding using X-ray spectroscopic probes is presented. Theoretical techniques to simulate XAS (X-ray absorption spectroscopy), XES (X-ray emission spectroscopy), RIXS (resonant inelastic X-ray scattering) and XPS (X-ray photoelectron spectroscopy) spectra have been developed and implemented within a density functional theory (DFT) framework. In combination with new experimental techniques, such as high-resolution XAS on liquid water under ambient conditions and XES on complicated surface adsorbates, new insight into *e.g.* hydrogen-bonded systems is obtained. For the (3×2) overlayer structure of glycine/Cu(110), earlier work has been extended to include adsorbate–adsorbate interactions. Structures are optimized for large cluster models and for periodic boundary conditions. It is found that specific features in the spectra arise from hydrogen-bonding interactions, which thus have important effects at the molecular-orbital level. XAS on liquid water shows a pronounced pre-edge feature with significant intensity, while the spectrum of ice shows only little intensity in this region. Theoretical spectrum calculations, based on instantaneous structures obtained from molecular-dynamics (MD) simulations, show that the pre-edge feature in the liquid is caused by water molecules with unsaturated hydrogen bonding. Some aspects of the theoretical simulations will be briefly discussed.

Keywords: water; hydrogen bonding; density functional theory (DFT); glycine/Cu(110); liquid XAS.

1. Introduction

The hydrogen bond represents one of the most important forms of intermolecular interaction. The cooperativity effect, *i.e.* that the effective dipole moment and hydrogen-bond (HB) strength are enhanced when the HB network is extended, is indicative of electronic structure changes upon coordination, but it is not clear that this could be directly measurable by electronic structure techniques. Indeed, the high vapour pressure of liquid water in combination with the UHV (ultra-high vacuum) experimental environment has long made high-resolution investigations of the electronic structure of bulk water problematic.

We have recently developed an experimental technique which resolves many of these difficulties; ambient-pressure ambient-temperature high-resolution measurements without differential pumping have thus become accessible. The key issue was the replacement of the vacuum environment by a helium atmosphere to reduce the partial pressure of water in the chamber; furthermore, by maintaining a flow of He gas through the chamber, most of the water vapour can be removed. The measurements are performed on a drop of liquid in a sample holder, which can be replaced without concern for maintaining the vacuum. This reduces sample preparation time substantially. From these types of measurements an increasing stream of data is emerging, which becomes a challenge to the theoreticians.

In recent theoretical developments, we have implemented techniques, within the gradient-corrected density functional theory (DFT) framework, to generate X-ray absorption (XA) and emission (XE, RIXS) spectra directly from optimized structures, including complicated adsorbates on computationally large cluster models. In treating liquid systems, however, a distribution of structures must be assumed and combinations of electronic structure and molecular-dynamics (MD) techniques are desired. In the present short overview, we will briefly describe the results obtained for a few hydrogen-bonded systems (liquid water, ice and chemisorbed glycine), the X-ray absorption spectra of which exhibit clear effects caused by the presence of the hydrogen bonds.

Spectrum calculations on a large number of different structural situations, from the MD simulations, combined with the experimental data leads to the suggestion that the high-intensity pre-edge peak observed for liquid water arises from water molecules with asymmetric coordination at the protons, *i.e.* broken donor hydrogen bonds. Similarly, for (3×2)glycine/Cu(110), we find certain features in the XA and XE spectra that cannot be reproduced theoretically for a single adsorbate on a cluster model, but which come into very good agreement with experiment when orbital interactions between adsorbates are included in more extended models.

2. Methods

2.1. Theoretical

The theoretical XA spectra were generated using the *deMon* program (Casida *et al.*, 1997), which implements the Kohn–Sham approach to DFT. Gradient-corrected exchange and correlation functionals (Perdew & Wang, 1986; Becke, 1988; Perdew, 1986) were used throughout. The procedure for computing the absorption spectra follows the static exchange (STEX) approximation, but uses a transition potential (half-occupied core level) for the determination of the excited states. The computational procedure is thus to determine the density for this (half-occupied) core-hole state in a good molecular basis set and then to diagonalize the Kohn–Sham matrix based on this density in a much larger basis set (double-basis-set technique). Typically, of the order of 200 additional diffuse functions are added to the excitation centre in this step.

The excitation energies are thus expressed as $\Delta E_{\text{exc}} = \varepsilon_f^T - \varepsilon_{1s}^T$, *i.e.* as differences between transition-state orbital energies; ε_{1s}^T corresponds to the 1s IP, and ε_f^T to the orbital energy of level *f*. As a result of the orthogonality, the oscillator strengths take the simple form of $(2/3)|\langle \varphi_{1s} | \hat{r} | \varphi_f \rangle|^2$. In the discrete part of the spectrum, the excitation energies and transition moments provide a true spectral representation and the spectrum is generated by applying a Gaussian broadening to the peaks. In the continuum part they provide a primitive spectrum for a Stieltjes imaging procedure in which a spectrum of order *N* is converted to a quadrature spectrum of order *n* ($n \ll N$) such that the first $2n$ spectral moments are reproduced. From the

quadrature spectrum, Stieltjes derivatives and the final Stieltjes imaged photoionization cross sections are obtained in the continuum (Langhoff, 1979). The resulting spectrum then gives a balanced treatment of valence, Rydberg and continuum excitations. A more detailed description can be found in works by *e.g.* Triguero *et al.* (1998) and Ågren *et al.* (1997).

2.1.1. Glycine/Cu(110). The structure of glycine/Cu(110) has been optimized using both cluster models and periodic plane-wave-based DFT techniques. In the cluster calculations, either one or two adsorbates were considered on cluster models with up to 36 copper atoms, in which the central 26 atoms were treated with all electrons included and the remaining were described by one-electron effective core potentials (ECP) (Mattsson *et al.*, 1987). All structural parameters of the adsorbate were optimized using energy gradients (Hasselström *et al.*, 1998); for the adsorbed dimer model, the geometry of the directly interacting substrate atoms was also optimized. The basis sets used were of triple-zeta plus polarization type for the adsorbate atoms and double-zeta plus polarization for the copper atoms. In the largest calculations, where three glycine molecules are adsorbed on a Cu₃₇ all-electron cluster model, the basis set on the copper is extended to quadruple-zeta for the 3*d* orbitals.

In order to determine the structure of the periodic overlayer unambiguously, we have extended our studies to consider periodic DFT calculations using a plane-wave basis. The periodic calculations (Hutter *et al.*, 1999) employ the free-energy density functional (Alavi *et al.*, 1994) and *k* points for a proper representation of the metal surface.

The Kohn–Sham orbitals are expanded in a plane-wave basis in combination with the pseudopotential approximation. We used dual-space pseudo potentials (Goedecker *et al.*, 1982), which for copper included 3*d*, 4*s* and 4*p* in the valence, and included plane waves up to a kinetic cut-off of 90 Ry.

The geometry optimizations were performed with a 2×2 Monkhorst–Pack mesh (Monkhorst & Pack, 1976) on a slab with three copper layers (7.67 × 7.23 Å in the plane and a 7.0 Å vacuum layer) containing two symmetry-related glycate molecules and 18 copper atoms. The calculations started from the geometry-optimized clean copper surface and a symmetrization of the hydrogen-bonded molecules on Cu(110) from the cluster calculations on the dimer model. Only the two lowest layers of copper atoms were held fixed.

2.1.2. Water. The experimental structure of ice *I_h* (assuming ordered hydrogen atoms) was used for the spectrum calculations, while for liquid water we have taken example structures from MD simulations, but no attempt was made to average the computed spectra based on the radial distribution function. The MD simulations were performed as classical constant-volume and -energy simulations (Allen & Tildesley, 1987) on a repeated cubic box containing 216 water molecules to model the liquid. The potential energy surface for the interactions between the water molecules was described by the OSS2 potential (Ojamäe *et al.*, 1998), which has been derived from *ab initio* calculations on protonated and neutral water clusters (Ojamäe *et al.*, 1998) and has been applied successfully in studies of such clusters (Ojamäe *et al.*, 1998; McDonald *et al.*, 1998). The model allows internal flexibility (O–H covalent bond stretching and H–O–H bending) and treats the electronic polarization of a molecule in a self-consistent manner through the polarizability of the oxygen ions. Polarization effects caused by both induced dipole moments and molecular distortion are thus taken into account. Long-range electrostatic interactions were included through the Ewald summation technique (Allen & Tildesley, 1987). The simulation was started from a well equilibrated sample at room temperature and was run for 4 ps using a time step of 0.1 fs.

2.1.3. Experimental. We obtained the O *K*-edge near-edge X-ray absorption fine structure (NEXAFS) spectra of water in liquid and gaseous forms using the Soft X-ray Endstation for Environmental Research (SXEER) and beamline 8.0 at the Advanced Light Source (ALS), Berkeley, USA. The beamline is equipped with a spherical-grating monochromator and a refocusing system providing a spot size of 100 × 100 μm. The measurement was performed with an overall resolution of 0.1 eV. The sample assembly in the SXEER is kept in He atmosphere at a pressure of 760 torr, and is separated from the high vacuum of the beamline by a 0.15 μm thin Si₃N₄ window. For NEXAFS measurements on liquid water, the sample was kept in a polypropylene straw with the surface of the water film near normal to the incident beam. This geometry minimizes any saturation effects in the spectra. The sample fluorescence was detected using a GaAs photodiode, kept at 90° to the incident beam to maximize the self-absorption of the fluorescence signal and thereby eliminating saturation effects in the NEXAFS spectra. An Si₃N₄ filter was also placed in front of the diode to avoid any charged particles reaching the detector. During the data collection, a constant flow of He gas was applied until the vapour contributions to the spectrum were negligible. The spectrum of water vapour was collected by stopping the He flow and moving the water sample away from the line of sight of the detector. The high-resolution ice spectrum was obtained from a carefully prepared overlayer (100 bilayers) of hexagonal ice on Pt(111). The ice film was grown by dosing D₂O using a pulsed gas delivery system. The exposure was controlled by the pulse duration, number of shots and the vapour pressure in the gas line and was made at a surface temperature of *T_s* = 125 K. The growth rate was 1–2 bilayers per minute. The measurements were performed with a slit opening of the monochromator providing a resolution of 0.1 eV.

The experiments on glycine/Cu(110) were also carried out at the IBM undulator beamline 8.0 at the ALS, using a modified spherical-grating monochromator. The experimental station consists of a multigrating grazing-incidence X-ray emission spectrometer with a movable multichannel plate-based detector, an electron energy analyser (Scienta SES-200) and a multichannel plate detector for NEXAFS measurements. Both the electron and X-ray spectrometers are rotatable around the axis of the incoming light. The details of the measurements can be found in previous publications (Hasselström *et al.*, 1998, 2000; Nyberg *et al.*, 2000).

3. Glycine adsorption on copper

There has recently been a strong interest in the glycine/Cu(110) chemisorption system, both because of the general interest in the interaction of biomaterials with metal implants and because glycine, as the simplest amino acid, is a prototype for these interactions. Glycine adsorbs in an ordered (3×2) structure at temperatures above

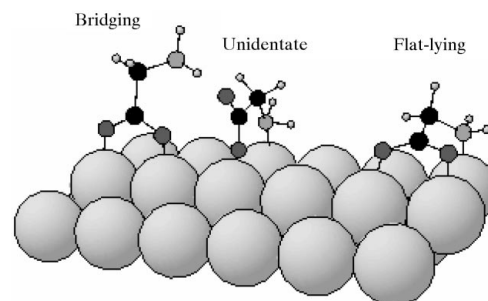


Figure 1
Different adsorption structures of glycine on Cu(110).

about 400 K, but the driving force behind this particular structure is one of the questions that has so far not been completely resolved.

The chemistry of glycine on Cu(110) has been studied by Barlow *et al.* (1998) using reflection absorption infrared spectroscopy (RAIRS). Several different structures were obtained, depending on the conditions; at the lowest temperatures (below 85 K) some of the glycine molecules were found to be still protonated, while at higher temperatures all adsorbates existed in the deprotonated form. The initial adsorption was determined to be bridging through the carboxylic group, but at higher coverages becoming unidentate with respect to the carboxylic group and bonding also with the amino end. Finally, annealing of this high-coverage phase to 430 K resulted in bridging bonding at the carboxylic group and bonding at both the amino and carboxylic ends (see Fig. 1); the resulting structural model is in agreement with the results of a photoelectron diffraction (Booth *et al.*, 1998) study and with our own analyses of the geometry on the basis of experimental XA and XE spectra and density functional calculations (Hasselström *et al.*, 1998, 2000; Nyberg *et al.*, 2000).

The bonding of glycine to the surface can be understood in terms of the bonding of the end-group building blocks, ammonia and formic acid. Similarly to formate (Karis *et al.*, 2000), the carboxylic group of glycine deprotonates spontaneously at rather low temperatures to form a bond with two (almost) equivalent oxygen atoms. The nitrogen binds with a lone pair sticking into the surface, similar to the case of ammonia (Hasselström *et al.*, 1999). The X-ray emission data of nitrogen show the same hybridization of p_z levels with the surface, which in the case of ammonia was interpreted as a $3a_1-4a_1$ hybridization with the metal. The carboxylic end of the molecule also forms bonds through hybridization of p_z levels with the surface, as was also the case for formate. One important difference here is that the carboxylic group of glycine has its plane not normal to the surface, as in the case of formate, but more parallel to it. For glycine, the π orbitals point directly into the surface and are responsible for the bonding, in contrast to the case of formate where the carboxylic π -type orbitals are not involved in the interaction with the surface. Still, a large part of the chemical bond between the carboxylic end of glycine and the surface should come from formation of an image charge in the surface, as found earlier in the case of the carboxylic acids (Karis *et al.*, 2000).

In our earlier theoretical investigations, we neglected the presence of the neighbouring adsorbates; the structure determined based on a single adsorbate as well as the computed XA and XE spectra for this

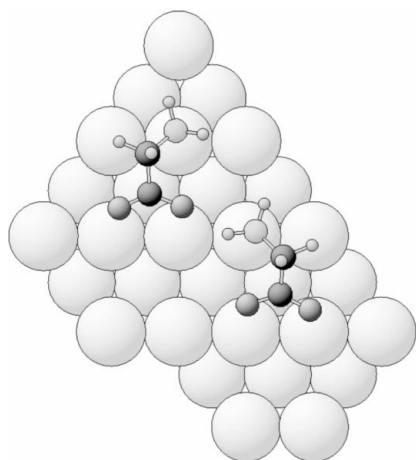


Figure 2
Optimized structure of two glycine molecules on a Cu_{36} cluster.

model were all in good overall agreement. However, in particular, the nitrogen XA spectrum showed features that could not be reproduced within this model. The geometrical structure of the overlayer makes it tempting to consider the formation of a hydrogen bond between the carboxylic and amino groups on neighbouring molecules (Fig. 2).

In order to examine this possibility, we have optimized the structure of two glycine molecules on a Cu_{36} cluster, in which some of the copper atoms directly involved in the bonding were relaxed; here a hydrogen atom on the amino group of one of the molecules is found to exhibit a typical hydrogen-bond distance (1.88 Å) to one of the oxygen atoms (see Fig. 2). The internal glycine structure obtained is, however, not very different from that obtained from the earlier optimization of a single glycine.

Using the cluster model in Fig. 2, our calculations show that, especially the XA spectra are very much affected by the inclusion of the hydrogen bond in the model. In Fig. 3, the experimental XA spectra of glycine are displayed, together with the calculated (hydrogen-bonded and single) spectra.

The improvements of the nitrogen XA spectra are obvious by inspection. In the previous investigations, in which only one glycine molecule was included in the model, we tentatively assigned the discrepancy between the calculated and the experimental XA data as due to difficulties in describing the typical Rydberg state interactions with the surface. In light of our new findings, we would like to ascribe these discrepancies to the lack of hydrogen-bonding interactions in the earlier model.

In the oxygen p_z spectrum, we find that a feature at around 535 eV appears in the extended model, also present in the experiment. In order to ascertain that this feature is the result of molecular orbital changes caused by the hydrogen-bond formation rather than by the slight change in geometry, the spectra were recomputed with the second glycine removed from the cluster. With only one glycine, in the same optimized structure, the additional peak disappears and it is thus clear that this feature mainly arises from direct orbital changes caused by the hydrogen-bond formation. Analysis shows that this feature is dominated by contributions from the oxygen atom directly involved in the hydrogen bond. In the computed hydrogen-bonded O

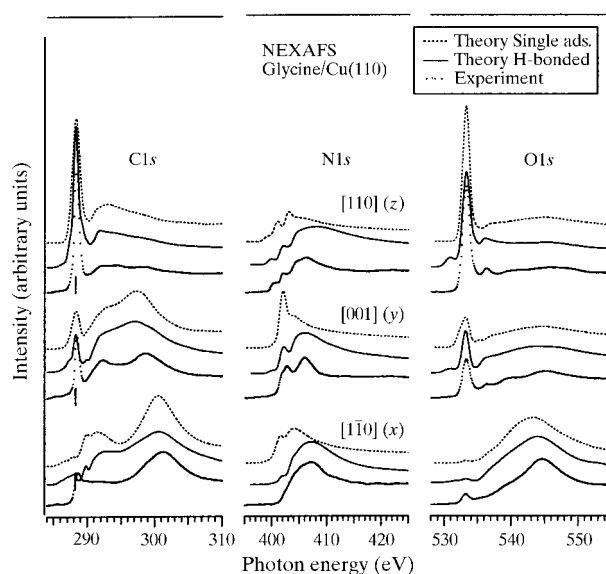


Figure 3
Theoretical X-ray absorption spectra for a single glycine and hydrogen-bonded glycine as compared to experiment. For each polarization direction, the order of the spectra is experiment (lower), theory hydrogen-bonded (middle) and theory single-adsorbate (upper).

p_z spectrum, we find an extra peak at about 530 eV, which is not present in the experiment. An analysis of the theoretical XA data shows that this feature is dominated by contributions from the oxygen atom which is not involved in the hydrogen bond to the amino end of the neighbouring molecule. Therefore, it seems that something is still missing in the description of this oxygen.

In order accurately to determine the structure of the ordered (3×2) overlayer of glycinate on Cu(110), we have complemented the cluster calculations with calculations under periodic boundary conditions, as described in §2. From the resulting structure, shown in Fig. 4, it is immediately apparent that the distance between the second oxygen and a proton in the neighbouring glycine CH_2 group is short enough (2.16 Å) that also this interaction should be considered in a model. The hydrogen-bond ($\text{N}-\text{H} \cdots \text{O}$) distance increases somewhat in the periodical description (1.96 Å) as compared to the length of 1.88 Å obtained from the cluster containing two glycine molecules. This is probably the result of the constraints imposed by the surroundings in the periodic case. These constraints could also cause the nitrogen atom to stay nearly on-top of the copper atom, which is not the case in the 2-glycine cluster description: displacements of 0.04 Å in the periodic and single-adsorbate cases compared to 0.32 Å for the dimer model. Interestingly, in the photoelectron diffraction investigation by Booth *et al.* (1998), the displacement was determined to be 0.24 Å.

Including this second hydrogen bond leads to consideration of a Cu_{37} all-electron cluster model with three glycines interacting through hydrogen bonding. These calculations become very time-consuming, but preliminary results for the oxygen spectra show that the small pre-edge feature in the [110] spectrum disappears and a near-perfect agreement with experiment is obtained. For nitrogen, the agreement is still very good, while the carbon spectra remain to be investigated.

The formation of intermolecular hydrogen bonds could thus explain the (3×2) structure as obtained from low-energy electron diffraction (LEED). The arrangement depicted in Fig. 4 (which is

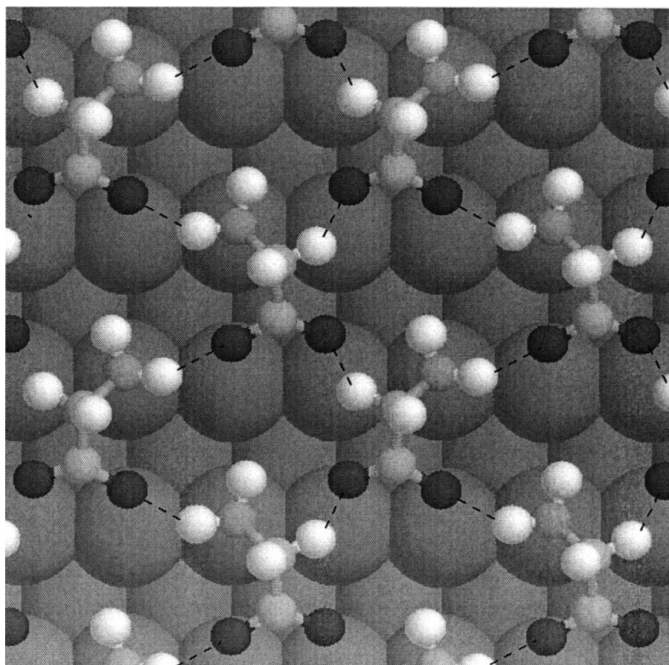


Figure 4
Optimized (3×2) structure for glycine on the surface.

consistent with the LEED data) is the only possibility to form hydrogen bonds involving both oxygen atoms on all of the adsorbates. The structure of glycine is mainly determined by the adsorbate–surface chemical bond, but the arrangement of glycine on the surface seems to be governed by the intermolecular hydrogen bonds. We further note that, given the appropriate model, the present computational techniques seem quite reliable in reproducing the electronic structure effects, as measured by XAS, even though generated by weak interactions such as the hydrogen bonds formed in the glycine overlayer.

4. Water

We have recently succeeded in measuring the near-edge XA spectrum of liquid water at high resolution (Myneni *et al.*, 2001) using the techniques described above. For comparison, new high-resolution spectra of ice I_h , grown as a thin film on Pt(111), were also obtained. The spectra are largely different in the pre-edge region around 535 eV (Myneni *et al.*, 2001). For the liquid, the pre-edge peak shows significant intensity, comparable to that of the main broad conduction band, while in the ice spectrum this intensity is very weak. The analysis of the contributions in this energy region shows that this intensity in the liquid is caused by the presence of water molecules with broken hydrogen bonds on the proton side (Myneni *et al.*, 2001). Fully coordinated water molecules have quasi-tetrahedral coordination similar to ice and the $2p$ character is shifted from the a_1 region into the conduction band. Breaking a hydrogen bond at the acceptor lone pair has only small effects on the orbital structure since there are no low-lying unoccupied molecular levels with which to mix; the lone pair is a fully occupied, out of (local) plane oxygen $2p$. At the proton side, the sensitivity is higher as a result of the availability of both bonding and antibonding O–H combinations. The oxygen contribution to the a_1 orbital contains both $2s$ and $2p$, while that to the b_1 orbital contains only $2p$. Thus, when the effective local C_{2v} symmetry is broken through loss of a donor bond, these symmetries can mix and the b_1 admixture enhances the intensity in the a_1 derived peak. This thus provides a direct electronic structure measure of the proportion of broken hydrogen bonds in the liquid (Myneni *et al.*, 2001).

In contrast to the case of glycine above, we must now model a system that does not have a specific structure. Energy minimization, which would give the 0 K structure, is not appropriate and we must find other techniques to generate suitable structures. We have thus combined MD simulations with the electronic structure calculations and use geometries sampled from the MD dumps. Because of the short time scale of the excitation, the use of frozen structures from individual time steps in the MD simulation corresponds directly to the characteristics of the experiment. The experimental spectrum should now be viewed as the sum of contributions from water molecules in coordination environments that follow a distribution function. To analyse the origin of the different features theoretically, we only need to study specific examples, but to reproduce the relative intensities, we need a sufficiently large number of spectrum calculations to sample the distribution function statistically and make reliable comparisons with the real distribution as viewed from the electronic structure. This is a formidable task and requires considerable speed-up and development of the computational procedure.

This work was supported by the Swedish Natural Science Research Council (NFR) and by the Göran Gustafsson Foundation for Research in Natural Science and Medicine. The ALS is supported by the US Department of Energy.

References

- Ågren, H., Carravetta, V., Vahtras, O. & Pettersson, L. (1997). *Theor. Chem. Acc.* **97**, 14–42.
- Alavi, A., Kohanoff, J., Parrinello, M. & Frenkel, D. (1994). *Phys. Rev. Lett.* **73**, 2599–2602.
- Allen, M. & Tildesley, D. (1987). *Computer Simulation of Liquids*. Oxford: Clarendon Press.
- Barlow, S., Kitching, K., Haq, S. & Richardson, N. (1998). *Surf. Sci.* **401**, 322–335.
- Becke, A. (1988). *Phys. Rev. A*, **38**, 3098–3100.
- Booth, N., Woodruff, D., Schaff, O., Giessel, T., Lindsay, R., Baumgartel, P. & Bradshaw, A. (1998). *Surf. Sci.* **397**, 258–269.
- Casida, M. E., Daul, C., Goursoot, A., Koester, A., Pettersson, L. G. M., Proynov, E., St-Amank, A., Salahub, D. R. (principle authors), Duärte, H., Godbout, N., Guan, J., Hermann, K., Jamorski, C., Leboeuf, M., Malkin, V., Malkina, O., Nyberg, M., Pedocchi, L., Sim, F., Triguero, L. & Vela, A. (contributing authors). (2000). *deMon Software*.
- Goedecker, S., Teter, M. & Hutter, J. (1982). *Phys. Rev. B*, **54**, 1703–1710.
- Hasselström, J., Föhlich, A., Karis, O., Weinelt, M., Wassdahl, N., Nilsson, A., Nyberg, M., Pettersson, L. G. M., Samant, M. G. & Stöhr, J. (1999). *J. Chem. Phys.* **110**, 4880–4890.
- Hasselström, J., Karis, O., Weinelt, M., Wassdahl, N., Nilsson, A., Nyberg, M., Pettersson, L. G. M., Samant, M. G. & Stöhr, J. (2000). *J. Phys. Chem. B*, **104**, 11480–11483.
- Hasselström, J., Karis, O., Weinelt, M., Wassdahl, N., Nilsson, A., Nyberg, M., Pettersson, L. G. M., Samant, M. G. & Stöhr, J. (1998). *Surf. Sci.* **407**, 221–236.
- Hutter, J., Alavi, A., Deutsch, T., Bernasconi, M., Goedecker, S., Marx, D., Tuckerman, M. & Parrinello, M. (1999). *CPMD code*, MPI für Festkörperforschung and IBM Zurich Research Laboratory.
- Karis, O., Hasselström, J., Wassdahl, N., Weinelt, M., Nilsson, A., Nyberg, M., Pettersson, L. G. M., Samant, M. & Stöhr, J. (2000). *J. Chem. Phys.* **112**, 8146–8155.
- Langhoff, P. W. (1979). *Electron Molecule and Photon Molecule Collisions*, edited by T. Rescigno, B. McKoy & B. Schneider, p. 183. New York: Plenum.
- Mattsson, A., Panas, I., Siegbahn, P., Wahlgren, U. & Åkeby, H. (1987). *Phys. Rev. B*, **36**, 7389–7401.
- McDonald, S., Ojamäe, L. & Singer, S. (1998). *J. Phys. Chem. A*, **102**, 2824–2832.
- Monkhorst, H. & Pack, J. (1976). *Phys. Rev. B*, **13**, 5188–5192.
- Myneni, S., Luo, Y., Näslund, L. Å., Ojamäe, L., Ogasawara, H., Pelmenchikov, A., Väterlein, P., Hoska, C., Pettersson, L. G. M. & Nilsson, A. (2001). To be published.
- Nyberg, M., Hasselström, J., Karis, O., Wassdahl, N., Weinelt, M., Nilsson, A., & Pettersson, L. G. M. (2000). *J. Chem. Phys.* **112**, 5420–5427.
- Ojamäe, L., Shavitt, I. & Singer, S. (1998). *J. Chem. Phys.* **109**, 5547–5564.
- Perdew, J. (1986). *Phys. Rev. B*, **34**, 7406..
- Perdew, J. & Wang, Y. (1986). *Phys. Rev. B*, **33**, 8800–8802.
- Triguero, L., Pettersson, L. & Ågren, H. (1998). *Phys. Rev. B*, **58**, 8097–8110.